Stall Delay and Leading-Edge Suction for a Pitching Airfoil with Trailing-Edge Flap

Guosheng He* and Julien Deparday*
Federal Institute of Technology Lausanne, CH-1015 Lausanne, Switzerland
Lars Siegel† and Arne Henning‡
DLR, German Aerospace Center, D-37073 Göttingen, Germany
and
Karen Mulleners§
Federal Institute of Technology Lausanne, CH-1015 Lausanne, Switzerland

https://doi.org/10.2514/1.J059719

The flow around a pitching NACA0015 airfoil with an oscillating trailing-edge flap is experimentally investigated to characterize the influence of the flap kinematics on the development of dynamic stall. We specifically focus on the timing of the stall development and critical values of the leading-edge suction parameter as potential stall triggers. In general, static or dynamic trailing-edge flap motions strongly affect the entire lift response but preserve the characteristic evolution of the leading-edge suction parameter. The influence of the flap on the critical values of the leading-edge suction parameter and their timing is more subtle. Variations in the magnitude of the leading-edge suction are related to the instantaneous geometric effective angle of attack. A thin-airfoil theory-based model that linearly superimposes the effect of the flap on the response for a fixed flap in its neutral position correctly predicts the maximum values of the leading-edge suction parameter. The timing at which these maxima are reached corresponds to the stall delay and is dominated by the prestall temporal evolution of the effective angle of attack. Our results suggest that dynamic stall development is governed by characteristic stall delays rather than critical values of the maximum leading-edge suction parameter.

I. Introduction

DYNAMIC stall refers to the phenomenon of unsteady separation occurring on airfoils undergoing time-varying motions. The dominant feature characterizing dynamic stall is the growth and shedding of a large-scale coherent dynamic stall vortex, after the airfoil angle of attack exceeds the static stall angle. The formation and convection of the dynamic stall vortex cause an overshoot of the lift, a delay in stall, and hysteresis of the lift history. Dynamic stall can lead to high aerodynamic loads or cause dangerous vibrations, which may result in a reduced performance or shortened life cycle of the structure. To protect the integrity and safety of the system, it is often desirable to mitigate or even eliminate the effects of dynamic stall. Popular methods to mitigate dynamic stall include boundary-layer suction or blowing [1–3], applying plasma actuators [4–6], leading-edge slats [7], deforming geometries [8], and trailing-edge flaps [9–11].

In potential flow theory, a deflection of the trailing-edge flap changes the camber of the airfoil, which changes the bound vorticity and the lift on the airfoil. If separation occurs either on the airfoil or on the flap, the flap no longer produces as much lift variation as predicted by the potential flow theory. However, that is not the case for a dynamic trailing-edge flap [12]. A dynamic trailing-edge flap can further increase the lift slope with respect to static measurements. After the flap motion stopped, the effectiveness would decrease to values consistent with steady-state measurements with separation. By taking into account the increased effectiveness of dynamic flaps, a better control of the unsteady lift can be achieved. Medina et al. [13,14] investigated the influence of a 50% flap that was rapidly deflected within a convective time scale. The front part of the wing in their study was fixed at 0 or 20 deg, which correspond to attached and separated flow conditions. The transient lift responded immediately to the fast movement of the flap, regardless of initial flow conditions. For separated flows, a rapid flap deflection in both directions perturbed the leading-edge shear-layer dynamics and caused it to roll up into a leading-edge vortex. The formation of this leading-edge vortex explains the additional lift variations generated by a dynamic flap motion that are absent for a static flap deflection.

The dynamic lift response of a fixed airfoil with an active flap was systematically investigated by Pohl et al. [15] at a high Reynolds number of $Re = 1.8 \times 10^6$. The airfoil was fixed at 0 or 12 deg while different flap motion profiles were employed to obtain dynamic lift variations. The motion profiles included sinusoidal oscillations, ramp up/ramp down, and random sequences. For high flap actuation speeds during the sinusoidal and ramp motions, hysteresis emerges in the lift history. Flap separation was observed for high deflection angles above 10 deg and could be completely avoided if the residence time of the flap above this threshold angle was reduced, indicating the importance of understanding characteristic dynamic stall response and relaxation time scales.

Dynamic trailing-edge flaps have also been used to control dynamic stall. In most of these studies, a pulselike actuation was used. The most important control parameters are the start time of the actuation with respect to the dynamic stall process, the actuation duration of the pulse, and the deflection amplitude of the flap. Gerontakos and Lee [16] tested the influence of all these parameters independently and quantified their influence on the dynamic stall lift and pitching moment, as well as the wake flow structures. An early but longer flap actuation in conjunction with an upward flap deflection would be more effective in reducing the nosedown pitching moment excursions. A parametric study of the flap actuation using a discrete vortex method revealed that only upward flap deflections would lead to the reduction of aerodynamic damping [10]. The optimum actuation proposed would start between the mean and maximum airfoil angles of attack and last

Presented as Paper 2020-0083 at the AIAA SciTech Forum, Orlando, FL, January 6–10, 2020.; received 23 April 2020; revision received 9 July 2020; accepted for publication 12 August 2020; published online 7 September 2020.

*Postdoctoral Researcher, EPFL-STI-IGM-UNFoLD, Institute of Mechanical Engineering, Station 9

†Doctoral Candidate, DLR-AS-BOA, Institute for Aerodynamics and Flow Technology (AS), Bunsenstrasse 10.

‡Team Leader Transport Systems, DLR-AS-BOA, Institute for Aerodynamics and Flow Technology (AS), Bunsenstrasse 10.

§Assistant Professor, EPFL-STI-IGM-UNFoLD, Institute of Mechanical Engineering, Station 9. Senior Member AIAA.

around one-third of the oscillation period. Active trailing-edge flaps also have the potential to serve as primary flight control and vibration reduction devices, as well as replace the conventional swash plate system in helicopters [17].

The studies on pulselike flap actuation are important in understanding the transient response of the loads on the airfoil and have demonstrated their effectiveness to mitigate gusts. But, some disturbances in practice are continuous in nature. The dynamic stall control adopting continuous flap motion is not as extensively studied in the literature. Krzysiak and Narkiewicz [18] measured the unsteady aerodynamic loads on a pitching airfoil with a trailing-edge flap deflecting twice as fast as the main airfoil. The influence of phase delay between airfoil pitching and flap deflection was considered. The higher harmonic oscillations of the flap lead to dual loops of the lift and moment polars. A phase shift between the airfoil and flap oscillation has a significant influence on the lift and pitching moment coefficients. When the angle of attack of the airfoil and flap deflection increase simultaneously, there is an increase of maximum lift coefficient; and when the two angles decrease simultaneously, the maximum lift coefficient decreases. Lee and Su [19] investigated the effects of a trailing-edge flap that is actuated at different start times and amplitudes. Here, a delayed start of the flap motion was compensated for by a faster flap deflection compared to the pitch rate of the oscillating airfoil to keep the oscillation periods the same for both components. Large changes in the dynamic load hysteresis loops were observed, but the formation and detachment of the dynamic stall vortex were largely unaffected by the flap deflection, regardless of the starting time of the flap actuation. The effectiveness of the trailing-edge flap control scheme was comparable to that obtained via a pulsed ramp flap motion.

An accurate way to predict the onset and growth of the dynamic stall vortex is essential for successful modeling of the dynamic stall process and the effectiveness of a trailing-edge flap. The leading-edge suction parameter was proposed as a criterion for the discrete vortex shedding from the leading edge [20,21]. For any airfoil and Reynolds number, they suggested the existence of a maximum allowed leading-edge suction or critical value of the leading-edge suction parameter, which is independent of the motion kinematics. A vortex will shed from the leading edge when the instantaneous leading-edge suction parameter exceeds that critical value. This augmented discrete vortex method using just a single empirical parameter (the critical leading-edge suction parameter value) is an elegant approach to predict the onset, growth, and termination of the leading-edge vortex and the unsteady aerodynamic responses for different airfoils and motion kinematics [22–25].

Past efforts have shown the potential to considerably affect the dynamic stall response of an airfoil by using a dynamic trailing-edge flap. In this study, we want to further explore the concept of a critical leading-edge suction parameter as a potential stall trigger or indicator for a range of dynamic stall scenarios created by a dynamic trailing-edge flap. We experimentally study the effect of a harmonically oscillating trailing-edge flap on a NACA0015 airfoil using time-resolved velocity field and surface pressure measurements. Our focus is on characterizing the influence of different phase shifts between the main airfoil and the flap oscillations on the evolution of the leading-edge suction parameter and the dynamic stall delay.

II. Experimental Setup

The experiment was conducted in a recirculating wind tunnel at the DLR, German Aerospace Center in Göttingen. The open jet test section of the tunnel has a nozzle end size of 0.75×1.05 m. The tunnel was operated at an incoming freestream velocity of $U_\infty = 30$ m/s. A NACA0015 airfoil was placed horizontally in the center of the test section. The span of the airfoil was 1.05 m, and the chord length was $c = 0.3$ m. The Reynolds number based on the chord length is $Re = 5.5 \times 10^5$.

A sketch of airfoil and the pitching mechanism is shown in Fig. 1. The airfoil was pitched around the quarter-chord axis ($0.25c$) and has a movable trailing-edge flap with the rotation axis at $0.7c$. Both the airfoil and the flap were three-dimensionally printed, and the surface was painted black to keep it smooth and to reduce the reflection of the laser light. The gap at the flap hinge between the main airfoil and the flap was covered with flexible tape to ensure a smooth transition on the surface. Preliminary tests with and without the tape revealed negligible influence of the tape and the gap. The main airfoil was connected to a Nanotec DB87L01 brushless dc motor using a stainless steel shaft. This motor, equipped with a planetary 25:1 gear, gives a rated torque output of 52.5 N/m. The flap was connected to a second brushless dc motor (Nanotec DB43C048030) using an aluminum alloy shaft. This flap motor is equipped with a planetary 20:1 gear and gives a rated torque output of 8.8 N/m. The flap motor and support were attached and fixed to the main airfoil shaft, and they move together with the main airfoil (Fig. 1a). The motions of the two motors were synchronized and individually controlled by a Galil DMC-4040 motion controller. The main airfoil was pitched around its static stall angle of $\alpha_0 = \alpha_{ss} = 20$ deg with an amplitude of $\alpha_1 = 8$ deg and a frequency of f_{osc}. The reduced frequency of $k = \pi f_{osc} c/U_\infty$ for the main airfoil for the presented data is 0.1. The flap is either fixed at angle $\beta \in \{-20, -10, 0, 10, 20\}$ deg or oscillated around its neutral position of $\beta_0 = 0$ deg with an amplitude of $\beta_1 = 20$ deg. The oscillation frequency of the flap equals the frequency of the main airfoil. The phase lag $\Delta\Phi$ between the trailing-edge flap and main airfoil oscillation is varied from $-\pi$ to π.

The unsteady airfoil surface pressure distribution is measured in the midspan section of the airfoil. A total of 36 differential pressure transducers (Endevco model 8510B-1) are buried inside the wing and connected to the surface pressure holes using plastic tubes with a 1 mm inner diameter and a length of less than 200 mm. The pressure

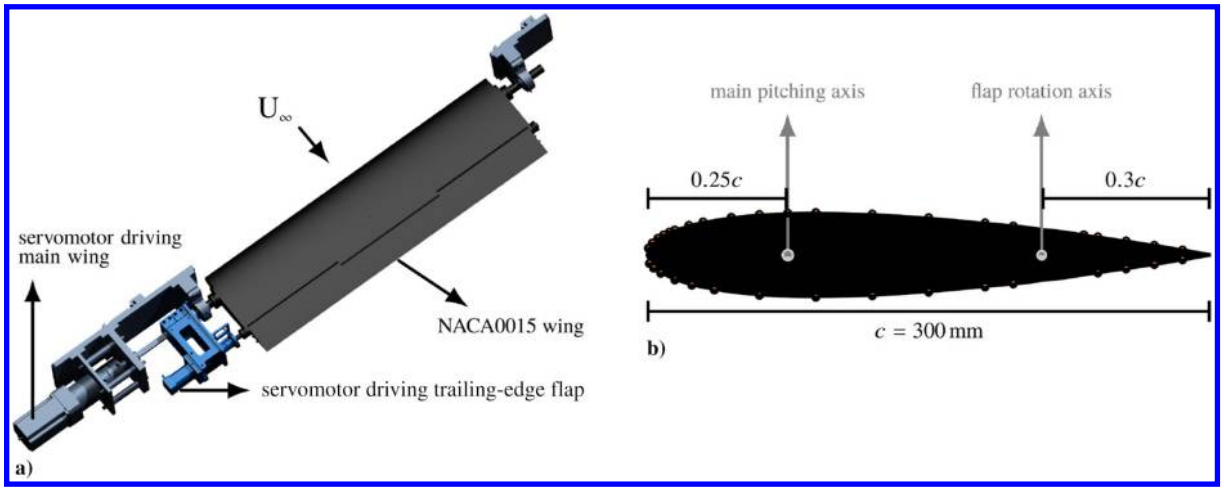

Fig. 1 Representations of a) pitching mechanism for the main airfoil and the trailing-edge flap, and b) positions of the pitching axes and the pressure transducers.

transducers have a measurement range of 0 to 6.89 kPa and a resonance frequency of 55 kHz. We have 20 pressure holes on the suction side and 16 along the pressure side (Fig. 1b). The usage of plastic tubes between the pressure holes and the transducers results in a cutoff frequency of 185 Hz for dynamic pressure measurements within a 3 dB magnification [26]. The sampling rate for pressure measurements is 20 kHz. Surface pressure data are recorded for 78 pitching cycles. The lift response is obtained by integrating the pressure distribution around the airfoil. The pressure data from the first 10% of the chord was used to calculate the leading-edge suction parameter using the procedure described in Ref. [25]. The leading-edge suction vector S_{LE} is calculated by integrating the pressure force based on the 13 pressure sensors in the front 10% of the airfoil. Note that S_{LE} is a nondimensional quantity obtained by normalizing the integral of the pressure measurements by $0.5\rho U_\infty^2 c$. The magnitude of the leading-edge suction vector is indicated by $|S_{\mathrm{LE}}|$ and its angle with respect to the incoming flow by λ. The experimental nondimensional leading-edge suction parameter is the projection of the leading-edge suction vector onto the chordwise direction:

$$A_{0,\mathrm{exp}} = \mathrm{sign}(S_{\mathrm{LE}})\sqrt{\frac{2}{\pi}|S_{\mathrm{LE}}|\cos(\lambda-\alpha)} \tag{1}$$

where α is the instantaneous angle of attack of the airfoil, and $\mathrm{sign}(S_{\mathrm{LE}})$ is negative when the suction vector is pointing downstream and positive when pointing upstream.

Two-dimensional particle image velocimetry (PIV) is used to measure the flowfield at the midspan of the airfoil. The flowfield is illuminated by a dual-pulsed Quantronix laser, and the particle images are recorded by a PCO DIMAX HS camera with a 1800×1600 pixel sensor. The camera is zoomed in around the leading edge, and the field of view covers the front 20% of the airfoil. The sampling rate for the PIV is 1.5 kHz. A multigrid algorithm was used to obtain the velocity vectors with the final window size of 48×48 pixels and 50% overlap yielding a physical grid resolution of 1.83 mm $=$ $0.0061c$ in the leading-edge region.

III. Results

When a trailing-edge flap is deflected, it changes the effective angle of attack and camber of the airfoil (Fig. 2). The effective angle of attack is defined as

$$\alpha_{\mathrm{eff}} = \alpha + \Delta\alpha = \alpha + \arctan\left(\frac{0.3\sin\beta}{0.7 + 0.3\cos\beta}\right) \tag{2}$$

for a flap with length of $0.3c$. Here, α indicates the angle of attack of the main wing and β is the flap angle deflection. We only take into account the purely geometric effect of the flap deflection and not its influence on the leading-edge stagnation point or the induced effects resulting from an unsteady pitch or flap angle variation. The flap angle β is defined as positive when it is deflected downward, increases the effective angle of attack, and leads to a positive camber y_c. When the flap angle is negative, the effective angle is smaller than the angle of attack of the main wing and the airfoil has negative camber (Fig. 2). The maximum camber is always located at the flap hinge and increases with flap angle according to

$$y_c = 0.7c\sin\Delta\alpha \tag{3}$$

For the maximum flap deflection of 20 deg, which we consider here, we find maximum values of $\Delta\alpha = 6$ deg and $y_c = 0.07c$.

A. Static Lift and Leading-Edge Suction Response

The static lift responses for fixed trailing-edge flap angles of $\beta \in \{-20, -10, 0, 10, 20\}$ deg are presented in Fig. 3a. The error bars represent the standard deviations of the signals at the static angles of attack and do refer to a measurement error, but they are a measure for the inherent fluctuations of the pressure signals due to flow unsteadiness. Without flap deflection, the airfoil is symmetric and generates zero lift at a zero angle of attack, has a lift slope of 0.87π before stall, and has a static stall angle of 20 deg. The lift slope is much lower than the theoretical value of 2π, and the stall angle is higher than expected from numerical simulation or measurements in closed test section

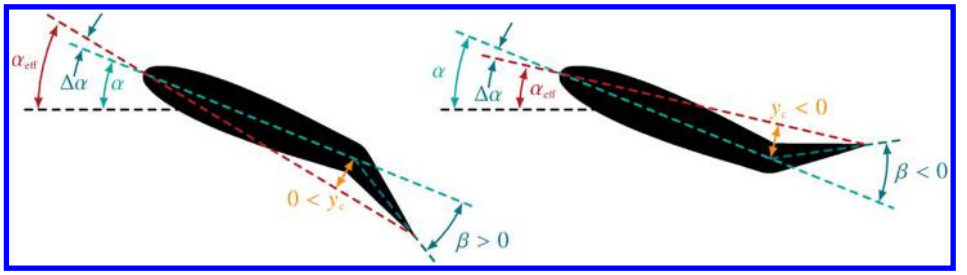

Fig. 2 Definition of the geometric effective angle of attack and camber as a result of the trailing-edge flap defection.

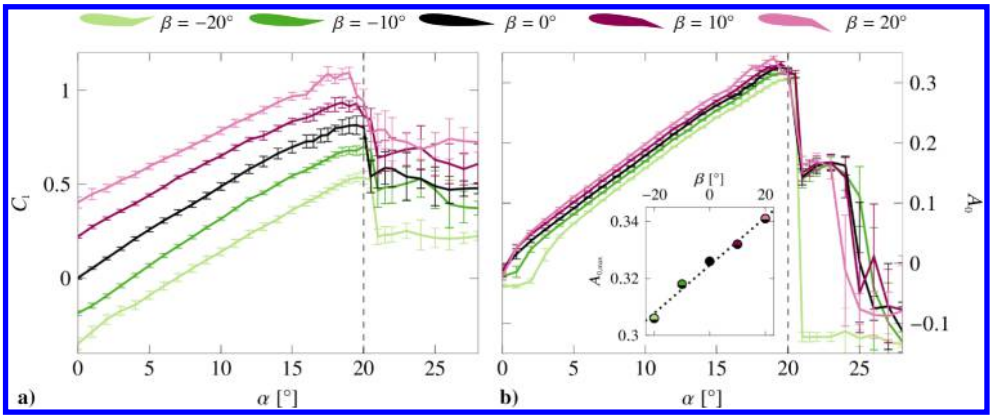

Fig. 3 Representations of a) static response of lift coefficient C_l and b) leading-edge suction parameter A_0 as a function of geometric angle of attack of main wing α for fixed deflections of trailing-edge flap $\beta \in \{-20, -10, 0, 10, 20\}$ deg. The inset in Fig. 3b shows variation of maximum leading-edge suction parameter with flap deflection angle.

facilities because our experiments have been conducted in a wind tunnel with an open test section. Wind-tunnel corrections for open jet flows by Ewald [27] allow us to compensate for the observed variation in the lift slope but are only applicable to fully attached flows and have not been applied to the presented data.

For positive flap angles, the effective camber increases and the static lift polar is shifted up along the lift axis. For negative flap angles, the effective camber decreases and the static lift polar is shifted down along the lift axis. The lift slopes before stall remain approximately the same for all flap angles, and the static stall angle based on the maximum lift peak varies only slightly from 20.5 to 19 deg between the largest negative and largest positive flap angles. The trailing-edge flap deflection substantially alters the lift generated but does not seem to have a major influence on the critical conditions that lead to stall.

In recent years, the leading-edge suction parameter has received renewed attention as a potential indicator and critical stall parameter [22–24]. In previous work [25], Deparday and Mulleners showed the increase of the critical leading-edge suction parameter with increasing unsteadiness of the pitching motion. Here, we want to build upon these efforts and further explore the influence of a trailing-edge flap deflection and motion on the critical leading-edge suction.

The static response of the leading-edge suction parameter A_0 as a function of the main wing angle of attack is presented in Fig. 3b. The leading-edge suction increases approximately linearly with angle of attack when the flow is attached. The rate of increase of the leading-edge suction is the same for all flap deflection angles, and curves have a clear drop off between $\alpha = 20$ deg and $\alpha = 21$ deg. The maximum value that the leading-edge suction parameter reaches increases linearly with increasing flap deflection angle (Fig. 3c). This maximum value is a measure for the maximum leading-edge adverse pressure gradient that the airfoil can sustain before stalling [20,28,29]. The influence of the flap defection on the static response of the leading-edge suction is considerably smaller than the influence on the lift coefficient. This suggests that the main difference in lift is not generated near the leading edge but distributed over the entire chord. As a consequence, the leading-edge adverse pressure gradient is only slightly affected and the critical leading-edge values and stall angles vary no more than 10% or 1 deg for flap deflections angles from $\beta = -20$ deg to 20 deg. But, the small variations we detect are consistent and indicate that a higher flap angle leads to a higher critical leading-edge suction value and a lower static stall angle.

B. Dynamic Lift Response for an Oscillating Trailing-Edge Flap

The dynamic lift responses for a sinusoidally oscillating airfoil with oscillating trailing-edge flap are summarized in Fig. 4. The temporal evolution of the effective angle of attack and phase-averaged lift coefficient are presented in Figs. 4a and 4b for different phase delays $\Delta\phi$ between the main wing and the flap oscillation. The line colors indicate the value of the phase delay. The bottom x axis shows the convective time with respect to the time at which the static stall angle of 20 deg has been exceeded. The top axes indicate the geometric angle of attack of the main wing and the time normalized by the pitching period. The main wing and the flap oscillate with the same frequency, and the pitching period starts when the main wing is at the minimum angle of attack. The dashed line represents the lift evolution for the airfoil with the flap fixed at 0 deg. The effective angle of attack is calculated according to Eq. (2). Negative phase delays correspond to motions where the flap motion leads the main wing motion such that the maximum effective angle is reached in the first half of the cycle. Positive phase delays correspond to motions where the flap motion lags the main wing motion such that the maximum effective angle is reached in the second half of the cycle. The motions are in phase when the main wing angle α and the flap angle β increase and decrease together such that they reach the highest possible effective angle of attack in the middle of the pitching cycle. The maximum and minimum values of the effective angle, respectively, decrease and increase with increasing phase shift,

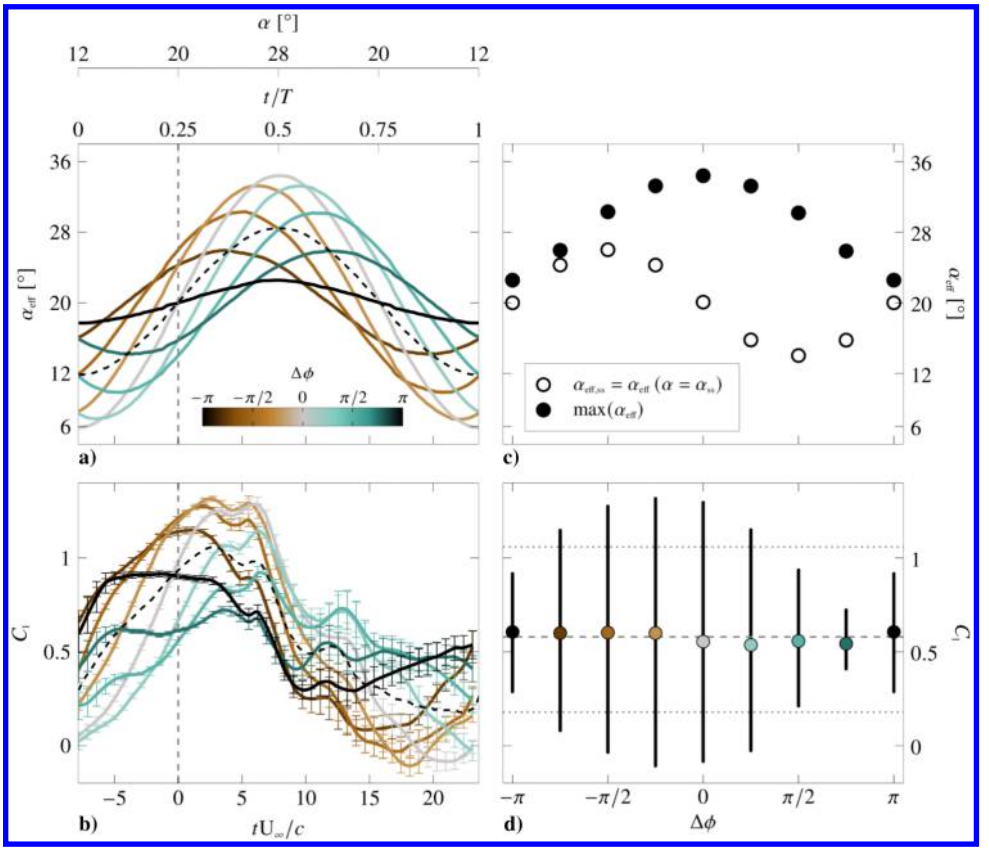

Fig. 4 Representations of a) temporal evolution of effective angle of attack α_{eff}, b) lift coefficient C_l for different phase delays $\Delta\phi$ between trailing-edge flap and main wing oscillation, c) maximum effective angle and effective angle at static stall for different phase delays, and d) time-averaged lift coefficient and C_l range spanned for different phase delays. Dashed and dotted lines represent time-averaged lift coefficient and range for motion with flap fixed at 0 deg.

leading to a decrease of the effective pitch angle-of-attack amplitude with increasing absolute value of the phase delay (Fig. 4c). The time-averaged mean effective angle remains at 20 deg for all motions, which corresponds to the static stall angle of attack α_{ss}. The effective angles of attack that are reached when the main wing angle exceeds the static stall angle are higher than 20 deg if the flap is leading the main wing, lower than 20 deg when the flap is lagging the main wing, and equal to 20 deg when the flap and the main wing are in or 180 deg out of phase (Fig. 4c).

The dynamic stall lift responses for the oscillating trailing-edge flap vary widely with the phase delay between the flap and the main wing. In general, the lift coefficient is higher in the first part of the cycles when the flow is attached and decreases during the second part of the cycle where increased values of the standard deviation, represented by the error bars, indicate flow separation. The error bars do not indicate experimental uncertainly or error here but are a measure for the inherent fluctuations of the pressure signals due to the unsteadiness of the flow and cycle-to-cycle variations [30,31]. In most cases, there are two peaks in the high angle-of-attack range ($24 \text{ deg} < \alpha < 28 \text{ deg}$). The first peak indicates the main dynamic stall lift overshoot that is reached when the shear layer starts to roll up into the primary dynamic stall vortex. The second peak is associated with the additional vortex lift due to the presence of the dynamic stall vortex on the airfoil. The time-averaged lift coefficient lies within $\bar{C}_{l,\text{noflap}} \pm 0.04$, with $\bar{C}_{l,\text{noflap}}$ as the time-averaged lift coefficient for the pitching motion with a fixed flap at 0 deg indicated by the dashed line in (Fig. 4b). The time-averaged lift values of the leading flap motions are slightly above the no-flap value, and the values of the lagging motions are slightly below. The vertical lines in Fig. 4d indicated the range of C_l values spanned by the phase-averaged dynamic stall curves. The range of lift values spanned by the motion with fixed flap at 0 deg is indicated by the dotted lines. The effective angle-of-attack amplitude decreases with increasing absolute value of the phase delay, leading to smaller fluctuations of the lift coefficient. The lift excursions for the motion with the flap leading by $\pi/4$ are highest, even though this motion covers the same effective angle-of-attack range as the motion with the flap lagging by $\pi/4$. The effective angles of attack during the first half of the cycle, and thus prestall, are higher for motions where the flap leads. This leads to higher prestall lift values but also a more severe lift breakdown during stall and a larger range of C_l values spanned within a pitching cycle. The lift response is influenced by the effective angle-of-attack amplitude as well as by the value of the effective angle of attack at prestall. The effective angle-of-attack amplitude is indicated by the maximum value of α_{eff}. The prestall values of the effective angle are represented by $\alpha_{\text{eff,ss}}$, which is the effective angle when the main airfoil is at the static stall angle α_{ss}.

C. Dynamic Leading-Edge Suction Response for an Oscillating Trailing-Edge Flap

To assess the stall onset and investigate the influence of the flap motion on the stall delay, we analyze the evolution and critical values of the leading-edge suction parameter (Fig. 5). The temporal evolution of the phase-averaged leading-edge suction parameter A_0 is presented in Fig. 5b for different phase delays between the flap and the main wing. The leading-edge suction parameter is more robust to oscillations of the trailing-edge flap than the lift coefficient. The phase-averaged evolution of the leading-edge suction follows the same evolution for all oscillating flap motions as for the case with the flap fixed at 0 deg, which is represented by the dashed line in Fig. 5b. In the beginning of the cycle, the leading-edge suction increases approximately linearly until about two to four convective time units after the static stall angle is exceeded. Within the next five to seven convective times, the values drop to a value of -0.13 and stay low for most of the second half of the cycle. Approximately five convective times before the end of the cycle, the leading-edge suction starts to recover and increases to its initial values. The variations between the responses for different phase delays are much smaller than the variations within a pitching cycle. Nevertheless,

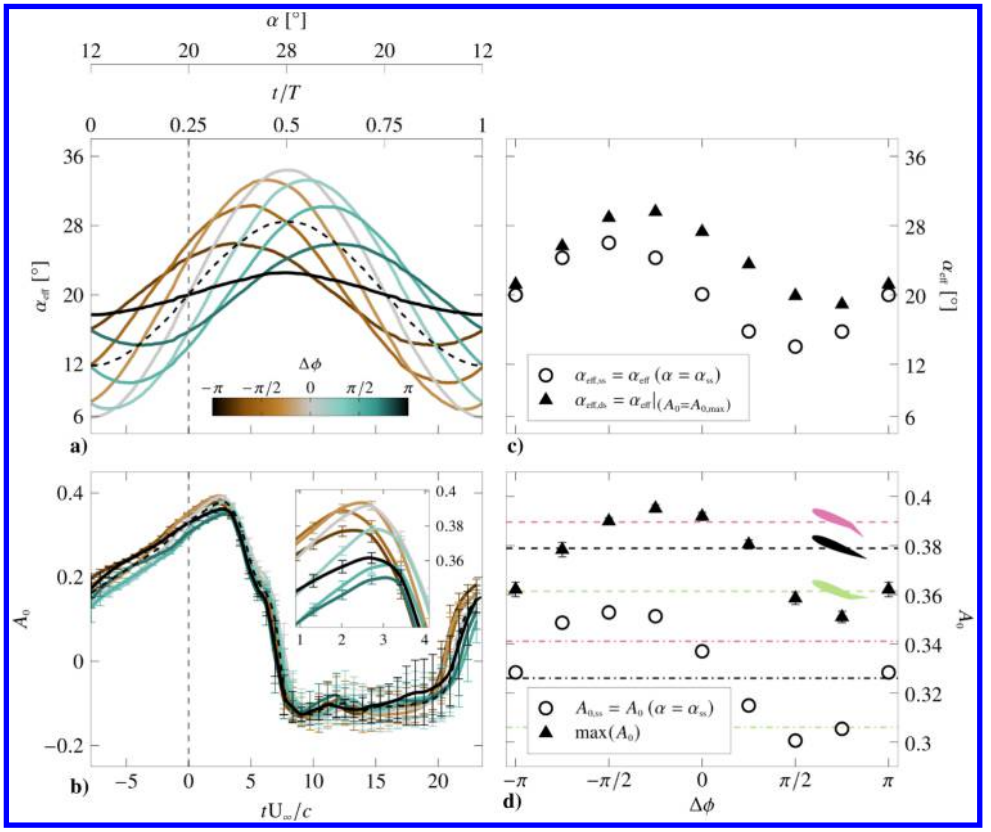

Fig. 5 Representations of a) temporal evolution of effective angle of attack α_{eff}, b) leading-edge suction parameter A_0 for different phase delays $\Delta\phi$ between trailing-edge flap and main wing oscillation, c) effective angle at static stall and dynamic stall for different phase delays, and d) A_0 at static and dynamic stall for different phase delays. Dashed lines represent maximum values of A_0 for a dynamically oscillating motion with flaps fixed at −20, 0, and 20 deg. Dashed–dotted lines represent maximum values of A_0 for static response of airfoil with flaps fixed at −20, 0, and 20 deg.

we can identify the influence of the phase delay on the leading-edge suction parameter (Fig. 5d). The triangular and circular symbols in Fig. 5d indicate, respectively, the maximum value of A_0 and its value at static stall. The dash–dotted lines represent the critical values of the static evolution of A_0 according to Fig. 3b, and the dashed lines represent the critical values of the dynamic evolution of A_0 for the same airfoil pitching motion with a fixed flap at $\beta = -20$, 0, and 20 deg.

The values of the leading-edge suction at the static stall angle vary with the effective angle at static stall (open symbols in Figs. 3c and 3d). The maximum and minimum values of $A_{0,ss}$ are found, respectively, for phase delays of $-\pi/2$ and $\pi/2$, which correspond to the motions with the highest and lowest effective angles of attack at the static stall angle. The values of $A_{0,ss}$ for the in-phase and 180 deg out-of-phase motions are close to the static values for the fixed flap at 0 deg. In all of these three cases, the effective angle of attack equals the main wing angle of attack for $\alpha = 20$ deg. Before dynamic stall, the leading-edge suction parameter is entirely driven by the instantaneous value of the effective angle of attack and is not influenced by the flap and wing dynamics or the history effects of the motion.

The maximum values of the leading-edge suction parameter and the corresponding effective angles of attack at which they occur are presented by the triangular symbols in Figs. 5c and 5d. The first important observation is the lack of a unique critical value of the leading-edge suction. A flap deviation and a flap motion both affect the maximum values of the leading-edge suction that can be obtained within a pitching cycle. The critical values for the various dynamic pitching oscillations are all higher than the maximum values for the static cases, which are indicated by the dashed–dotted lines in Fig. 5d. The overall highest and lowest maximum values are observed for phase delays of $-\pi/4$ and $3\pi/4$, respectively. The values of $A_{0,max}$ for these phase shifts are even higher (respectively, lower) than the critical values measured for oscillations with fixed flap angles of 20 and -20 deg, which are indicated by the dashed lines in Fig. 5d. The higher values of $A_{0,max}$ generally occur at higher effective angle of attacks. The correlation between the maximum leading-edge suction and the effective angles of attack at static stall, at dynamic stall, and the maximum effective angle are summarized in Fig. 6. Here, we refer to dynamic stall as the moment at which the maximum leading-edge suction parameter is reached, which coincides with the start of the rollup of the shear layer according to previous work by Deparday and Mulleners [25].

For a given absolute value of phase shift $|\Delta\phi|$ between the main wing and the flap oscillation, the same values of $\alpha_{eff,max}$ are obtained but the maximum values of A_0 are higher if the flap motion is leading ($\Delta\phi < 0$) than when the flap motion is lagging ($\Delta\phi > 0$) (Figs. 6a and 6c). The maximum effective angle and its value at static stall are not sufficient to predict the critical leading-edge suction. In Fig. 6b, we do observe a linear relationship between $A_{0,max}$ and the corresponding effective angle of attack at the instant the leading-edge suction parameter reaches it maximum value. Unless we know in advance at what angle dynamic stall occurs, this result does not allow us to predict the critical leading-edge suction. It merely shows that dynamic stall occurs at higher effective angles of attack if the critical maximum value of the leading-edge suction is higher. The question that remains is what causes the critical leading-edge suction parameter to be increased for certain flap motions or what causes dynamic stall to be delayed to higher effective angles of attack in these cases. To answer these questions, we will focus next on the stall delay.

D. Variations of the Dynamic Stall Delay

A dynamic stall delay of $\Delta t U_\infty/c$ is determined here as the convective time delay between the moment the main wing exceeds the static stall angle and the moment $A_{0,max}$ is reached. This corresponds to the duration of the primary stall development stage according to the nomenclature introduced in previous work by Deparday and Mulleners [25] and Mulleners and Raffel [32]. During this first stage, the shear layer grows in wall-normal direction. It is followed by a second stage during which the shear layer rolls up and forms the primary stall vortex. The second stage ends with the separation of the primary stall vortex, and its duration is related to a vortex formation time that is independent of the pitching motions kinematics.

The calculated values of the stall delay are presented in Fig. 7 versus phase shift, the maximum value of the leading-edge suction parameter, and the effective angle of attack at static stall $\alpha_{eff,ss}$. The stall delay for a leading flap motion is generally lower than for a lagging flap motion, and there is no injective functional relationship between the stall delay and the critical leading-edge suction parameter (Figs. 7a and 7b). The stall delay is best described in terms of the

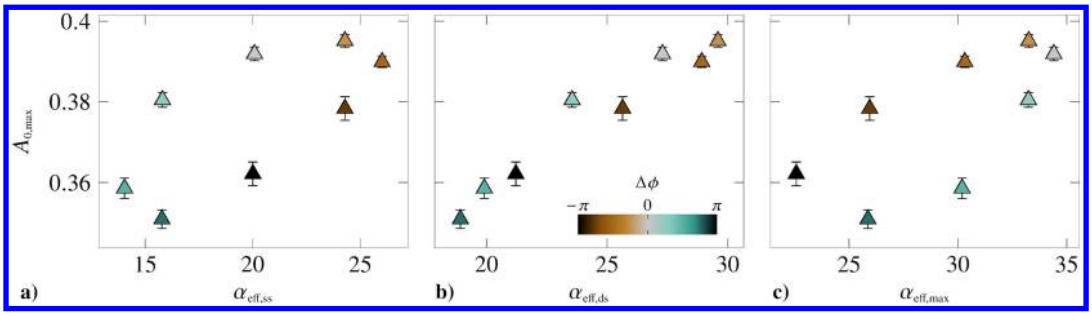

Fig. 6 Representations of a) maximum value of leading-edge suction parameter versus effective angle of attack at static stall $\alpha_{eff,ss}$, b) effective angle of attack at dynamic stall $\alpha_{eff,ds}$, and c) maximum value of the effective angle of attack $\alpha_{eff,max}$ for different phase shifts.

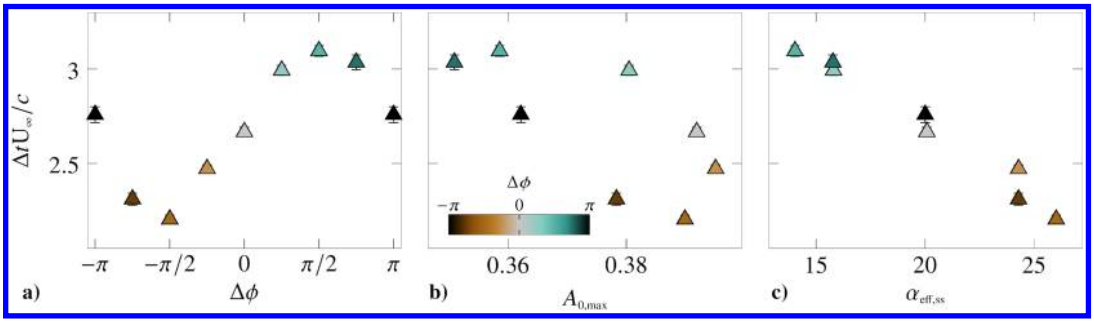

Fig. 7 Representations of a) nondimensional dynamic stall delay versus phase shift, b) maximum value of leading-edge suction parameter, and c) effective angle of attack at static stall.

effective angle of attack at static stall and decreases approximately linearly with increasing $\alpha_{\text{eff,ss}}$ (Fig. 7c). Higher values of $\alpha_{\text{eff,ss}}$ also lead to higher prestall lift values (Figs. 4c and 4d) and higher values of the leading-edge suction parameter at static stall (Figs. 5c and 5d).

The aforementioned findings suggest that the effective angle at static stall is a measure for the vorticity generated at the airfoil's surface that will accumulate in the shear layer. Higher values of $\alpha_{\text{eff,ss}}$ yield stronger shear layers that will start to roll up more quickly, resulting in a shorter stall delay. To corroborate this conclusion, we calculated the evolution of the leading-edge circulation in the front 10% of the airfoil. The results are summarized in Fig. 8. The integration area for the leading-edge circulation Γ_{LE} is indicated in Fig. 8a by the colored rectangle. The area covers the first 10% of the airfoil's suction region, starting from the leading-edge stagnation point. The position of the leading-edge stagnation point is determined as the extrapolated intersection of the stagnation line and the airfoil surface. The stagnation line is the ridge of the positive finite-time Lyapunov exponent in the leading-edge region. The circulation is calculated by integrating the tangential velocity along the edges of our rectangle. For different angles of attack, the size of the integration box is kept constant. The bottom of the box is aligned with the location of the leading-edge stagnation point. The calculation is performed on the instantaneous PIV data, and this information is then phase averaged. The resulting phase-averaged circulation and its standard deviation are shown in Fig. 8b. The temporal evolution of the phase-averaged leading-edge circulation values are presented in Fig. 8b for different phase shifts of the flap motion. The dashed line indicates the results of the oscillation with a fixed flap at 0 deg. The flap motions have a measurable influence on the leading-edge circulation but the general evolution is similar for all flap motions. The circulation increases in the first part of the cycle and reaches a maximum value shortly after $A_{0,\text{max}}$ is reached, which is indicated by the gray shaded region. Thereafter, the circulation drops rapidly for all cases down to the same value of approximately 1.2.

Characteristic values of leading-edge circulation at static and dynamic stall are presented in Fig. 8c versus phase shift and in Fig. 8d versus the corresponding effective angles of attack when the values are extracted. The leading-edge circulation values at static and dynamic stall are higher when the flap motion leads than when the flap motion lags. More generally, the leading-edge circulation increases approximately linearly with increasing effective angle of attack for the values extracted at static and dynamic stall. This confirms our previous conclusion that a higher effective angle at static stall results in higher leading-edge circulation, which then leads to a higher leading-edge suction parameter and lift. The stronger shear layer also promotes the rolling up of the shear layer and results in a shorter stall delay.

E. Thin-Airfoil Theory-Based Model

The experimental results for the leading-edge suction parameter suggest that the A_0 is primarily driven by the instantaneous values of the effective angle of attack. If this is indeed the case, we should be able to predict the influence of a trailing-edge flap motion based on thin-airfoil theory. According to thin-airfoil theory, the influence of a trailing-edge flap on the leading-edge suction parameter can be estimated by a superposition of the solution for the airfoil without the flap and the solution for the isolated flap of $A_0 = A_{0,\text{noflap}} + A_{0,\text{flap}}$ [33]. The solution for the flap is given by

$$A_{0,\text{flap}} = K_f \tan\beta \tag{4}$$

with β as the flap angle and

$$K_f = 1 - \Phi/\pi \tag{5}$$

where Φ is the chord-normalized hinge position of the trailing-edge flap of length l_{flap} defined such that

$$1 - l_{\text{flap}} = \frac{1}{2}(1 - \cos\Phi) \tag{6}$$

For the given geometry with $l_{\text{flap}} = 0.3$, we obtain $K_{\text{f}} = 0.37$.

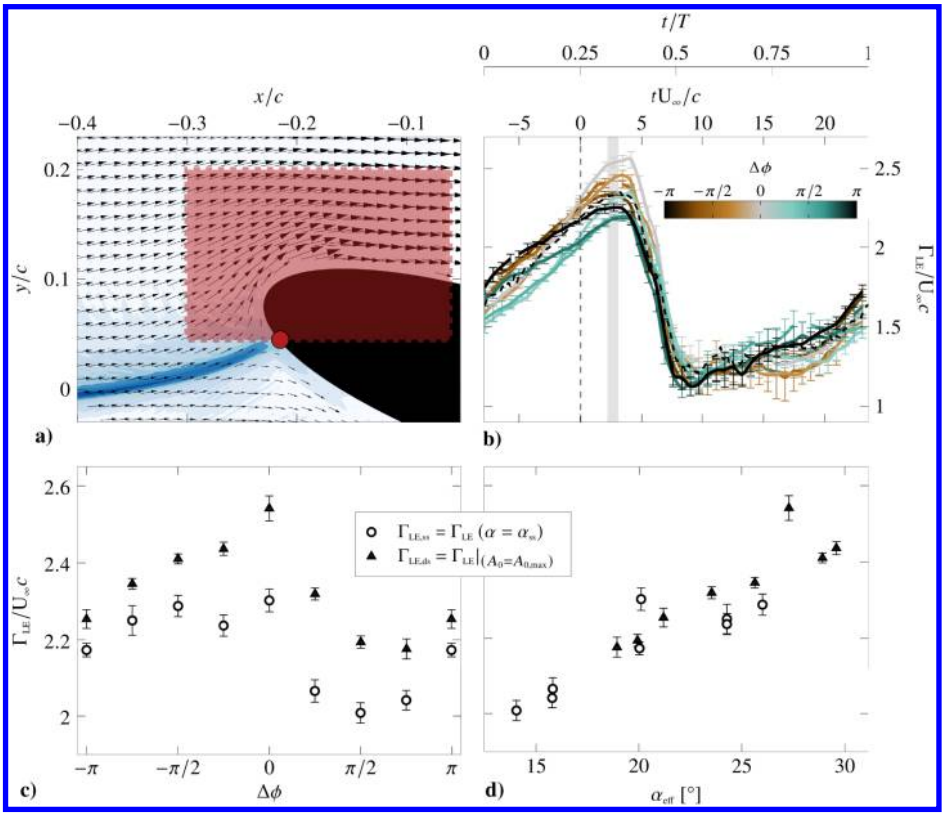

Fig. 8 Representations of a) integration region for leading-edge circulation; b) temporal evolution of leading-edge circulation; c) variation of leading-edge circulation values at static and dynamic stall versus phase shift between flap and main wing oscillation; and d) dynamic stall versus corresponding effective angle of attack.

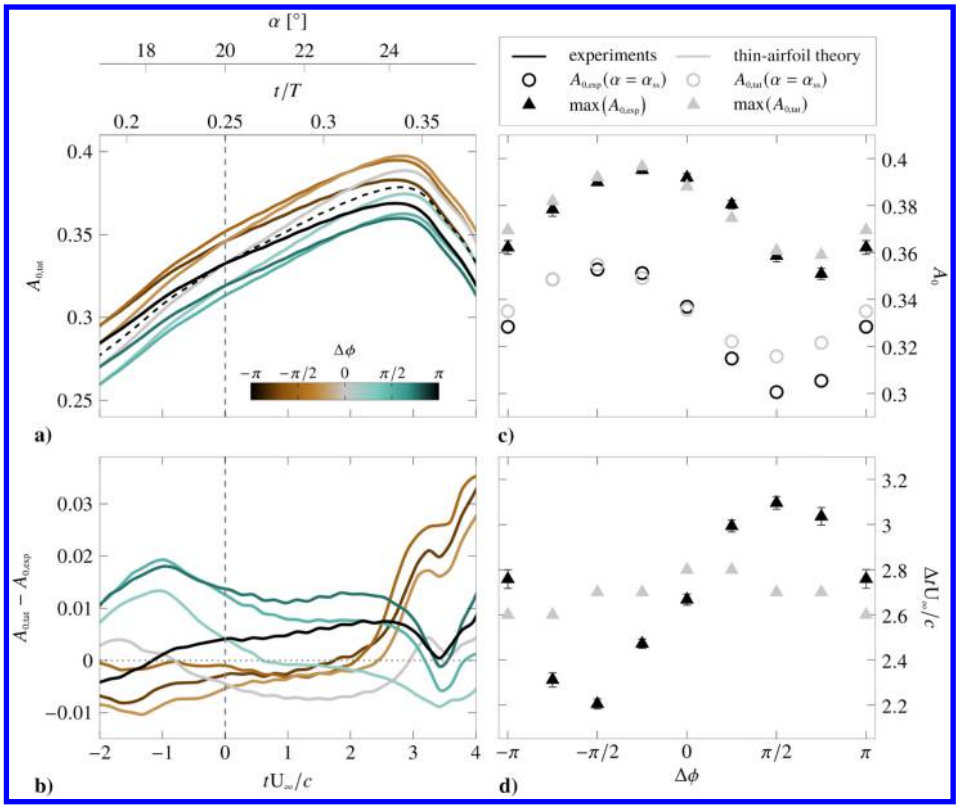

Fig. 9 Representations of a) evolution of leading-edge suction parameter based on thin-airfoil theory, b) deviation between model estimate and experimental values, c) comparison of experimental and theoretical values of A_0 at static stall and maximum values, and d) comparison of timing of experimental and theoretical maxima A_0.

We can also estimate the coefficient K_f from the static experimental results of the leading-edge suction parameter as a function of angle of attack (Fig. 3b). The vertical shift of the static curves for the fixed flap angles $\beta \in \{-20, -10, 10, 20\}$ deg with respect to the results for the case with $\beta = 0$ deg should be equal to $K_f \tan\beta$. By linearly fitting the prestall static A_0 versus α for the different fixed β values, we obtain an experimental coefficient of $K_{f,\text{exp}} = 0.053$, which is an order of magnitude lower than the coefficient calculated directly from the geometric parameters of $K_{f,\text{geo}} = 0.37$. The difference is attributed to the influence of the open jet test section and relative thickness of our airfoil.

We now use the flap coefficient of $K_{f,\text{exp}} = 0.053$ to obtain a first-order estimate of the influence of the flap motion on the leading-edge suction parameter by adding the contribution of $K_{f,\text{exp}} \tan\beta$ to the experimental results for the pitching motion with a fixed flap at 0 deg. The results of the thin-airfoil theory-based estimates and their deviation with respect to the experimental results are presented in Figs. 9a and 9b. We focus here only on the stall development part of the cycle. In general, the deviations between the experimental and theoretical results are less than 5% of the maximum A_0 value during prestall. The thin-airfoil model tends to underestimate the leading-edge suction parameter when the flap motion is leading and tends to overestimate when the flap motion is lagging with respect to the main wing motion. The error is lower for the leading flap motion. The estimated values at static stall and the maximum values of A_0 are well predicted by the thin-airfoil model and correctly reflect the influence of the flap motion (Fig. 9c). The timing of the maximum leading-edge suction (what we referred to as the stall delay) is not captured by the model. The timing based on the thin-airfoil model fluctuates around the experimental values found for the in-phase and 180 deg out-of-phase motions. The experimentally observed variations for the other phase shifts are not captured by the theoretical model. The thin-airfoil theory-based model only takes into account the instantaneous flap angles and does not consider any influence of the pitch rate or the history of the flap motion. The value of the leading-edge suction is primarily driven by the instantaneous effective angle of attack (Fig. 6b) and can be predicted by the thin-airfoil approach suggested here. The dynamic stall delay is strongly influenced by the prestall evolution of the effective angle of attack and not just the instantaneous values (Fig. 7c), and it cannot be predicted by this simple model. These results further support the idea that dynamic stall development is governed by critical stall delays rather than a critical maximum leading-edge suction parameter.

IV. Conclusions

The flow around a pitching NACA0015 airfoil with an oscillating trailing-edge flap is investigated using two-dimensional time-resolved particle image velocimetry and surface pressure measurements. The airfoil pitches around its static stall angle of attack, and the flap either oscillates with the same frequency as the main wing around its neutral position or is fixed at a constant deflection angle. The phase shift between the oscillation of the flap and the main wing is varied to create different temporal evolutions of the geometric effective angle of attack. The objective of the study is to characterize the influence of the trailing-edge flap kinematics on the development of dynamic stall. We specifically focus on the timing of the stall development and on the critical values of the leading-edge suction parameter as a potential stall trigger.

A static or dynamic trailing-edge flap motion significantly affects the static and dynamic stall lift responses but preserves the characteristic evolution of the leading-edge suction parameter. Subtle variations of the magnitude of the leading-edge suction are linearly related to the static flap defection angles or the instantaneous effective angle of attack at static or dynamic stall. Higher effective angles lead to higher values of the leading-edge suction parameter. A thin-airfoil theory-based model that linearly superimposes the effect of the flap on the response for a fixed flap in its neutral position correctly predicts the maximum values of the leading-edge suction parameter.

The moment in time at which the maximum leading-edge suction parameter is reached coincides with the start of the rollup of the shear

layer and is considered to mark dynamic stall onset here. Its time delay with respect to the moment at which the static stall angle is exceeded is referred to as the dynamic stall delay. The stall delay is not determined solely by the instantaneous effective angle but is influenced by the flap dynamics and the prestall temporal evolution of the effective angle of attack. For the trailing-edge flap oscillations considered here, the stall delay is best described in terms of the effective angle of attack at static stall and decreases linearly with increasing $\alpha_{\mathrm{eff,ss}}$. The decrease in the stall delay is due to an increase in the production of vorticity at the airfoil's surface for higher prestall effective angles of attack. This leads to a stronger shear layer that will start to roll up more quickly, resulting in a shorter stall delay. The maximum leading-edge suction value at dynamic stall is given by the instantaneous effective angle at the end of the stall delay. Dynamic stall development is thus governed by critical stall delays rather than a critical maximum leading-edge suction parameter.

Acknowledgments

The work presented is supported by the Swiss national science foundation Lead Agency program under grant number 200021E-169841 and by SNSF Assistant Professor energy grant number PYAPP2_173652. We thank Sabrina Henne and the DLR, German Aerospace Center staff for their assistance and support during the measurement campaign and the Federal Institute of Technology Lausanne mechanics workshop (in particular, Marc Jeanneret) for their invaluable support and advice for the design and construction of the pitching airfoil test rig.

References

[1] Carr, L. W., "Progress in Analysis and Prediction of Dynamic Stall," *Journal of Aircraft*, Vol. 25, No. 1, 1988, pp. 6–17. https://doi.org/10.2514/3.45534

[2] Alrefai, M., and Acharya, M., "Controlled Leading-Edge Suction for Management of Unsteady Separation over Pitching Airfoils," *AIAA Journal*, Vol. 34, No. 11, 1996, pp. 2327–2336. https://doi.org/10.2514/3.13398

[3] Karim, M. A., and Acharya, M., "Suppression of Dynamic-Stall Vortices over Pitching Airfoils by Leading-Edge Suction," *AIAA Journal*, Vol. 32, No. 8, 1994, pp. 1647–1655. https://doi.org/10.2514/3.12155

[4] Fukumoto, H., Aono, H., Watanabe, T., Tanaka, M., Matsuda, H., Osako, T., Nonomura, T., Oyama, A., and Fujii, K., "Control of Dynamic Flowfield Around a Pitching NACA633-618 Airfoil by a DBD Plasma Actuator," *International Journal of Heat and Fluid Flow*, Vol. 62, Dec. 2016, pp. 10–23. https://doi.org/10.1016/j.ijheatfluidflow.2016.10.012

[5] Iwasaki, Y., Nonomura, T., Nankai, K., Asai, K., Kanno, S., Suzuki, K., Komuro, A., Ando, A., Takashima, K., Kaneko, T., Yasuda, H., Hayama, K., Tsujiuchi, T., Nakajima, T., and Nakakita, K., "Dynamic Stall Control Around Practical Airfoil Using Nanosecond-Pulse-Driven Dielectric Barrier Discharge Plasma Actuators," *Energies*, Vol. 13, No. 6, 2020, Paper 1376. https://doi.org/10.3390/en13061376

[6] Singhal, A., Castañeda, D., Webb, N., and Samimy, M., "Control of Dynamic Stall over a NACA 0015 Airfoil Using Plasma Actuators," *AIAA Journal*, Vol. 56, No. 1, 2018, pp. 78–89. https://doi.org/10.2514/1.J056071

[7] Yu, Y. H., Lee, S., McAlister, K. W., Tung, C., and Wang, C. M., "Dynamic Stall Control for Advanced Rotorcraft Application," *AIAA Journal*, Vol. 33, No. 2, 1995, pp. 289–295. https://doi.org/10.2514/3.12496

[8] Chandrasekhara, M. S., Wilder, M. C., and Carr, L. W., "Unsteady Stall Control Using Dynamically Deforming Airfoils," *AIAA Journal*, Vol. 36, No. 10, 1998, pp. 1792–1800. https://doi.org/10.2514/2.294

[9] Kim, J. S., Smith, E. C., and Wang, K. W., "Active Load Control of an Articulated Composite Rotor Blade via Dual Trailing Edge Flaps," *44th AIAA/ASME/ASCE/AHS/ASC Structures, Structural Dynamics, and Materials Conference*, AIAA Paper 2003-1543, 2003. https://doi.org/10.2514/6.2003-1543

[10] Feszty, D., Gillies, E. A., and Vezza, M., "Alleviation of Airfoil Dynamic Stall Moments via Trailing-Edge-Flap Flow Control," *AIAA Journal*, Vol. 42, No. 1, 2004, pp. 17–25. https://doi.org/10.2514/1.853

[11] Gerontakos, P., and Lee, T., "Trailing-Edge Flap Control of Dynamic Pitching Moment," *AIAA Journal*, Vol. 45, No. 7, 2007, pp. 1688–1694. https://doi.org/10.2514/1.27577

[12] Rennie, R. M., and Jumper, E. J., "Experimental Measurements of Dynamic Control Surface Effectiveness," *Journal of Aircraft*, Vol. 33, No. 5, 1996, pp. 880–887. https://doi.org/10.2514/3.47030

[13] Medina, A., Ol, M. V., Mancini, P., and Jones, A., "Revisiting Conventional Flaps at High Deflection Rate," *AIAA Journal*, Vol. 55, No. 8, 2017, pp. 2676–2685. https://doi.org/10.2514/1.J055754

[14] Medina, A., Hemati, M. S., and Rockwood, M., "Separated Flow Response to Rapid Flap Deflection," *AIAA Journal*, Vol. 58, No. 4, 2020, pp. 1446–1457. https://doi.org/10.2514/1.J058367

[15] Pohl, J., Semaan, R., and Jones, A. R., "Dynamic Lift Measurements on an Airfoil with Periodic Flap Motion at High Reynolds Number," *AIAA Scitech 2019 Forum*, AIAA Paper 2019-1396, 2019. https://doi.org/10.2514/6.2019-1396

[16] Gerontakos, P., and Lee, T., "Dynamic Stall Flow Control via a Trailing-Edge Flap," *AIAA Journal*, Vol. 44, No. 3, 2006, pp. 469–480. https://doi.org/10.2514/1.17263

[17] Shen, J., Yang, M., and Chopra, I., "Swashplateless Helicopter Rotor with Trailing-Edge Flaps for Flight and Vibration Control," *Journal of Aircraft*, Vol. 43, No. 2, 2006, pp. 346–352. https://doi.org/10.2514/1.14634

[18] Krzysiak, A., and Narkiewicz, J., "Aerodynamic Loads on Airfoil with Trailing-Edge Flap Pitching with Different Frequencies," *Journal of Aircraft*, Vol. 43, No. 2, 2006, pp. 407–418. https://doi.org/10.2514/1.15597

[19] Lee, T., and Su, Y. Y., "Unsteady Airfoil with a Harmonically Deflected Trailing-Edge Flap," *Journal of Fluids and Structures*, Vol. 27, No. 8, 2011, pp. 1411–1424. https://doi.org/10.1016/j.jfluidstructs.2011.06.008

[20] Ramesh, K., Gopalarathnam, A., Edwards, J. R., Ol, M. V., and Granlund, K., "An Unsteady Airfoil Theory Applied to Pitching Motions Validated Against Experiment and Computation," *Theoretical and Computational Fluid Dynamics*, Vol. 27, No. 6, 2013, pp. 843–864. https://doi.org/10.1007/s00162-012-0292-8

[21] Ramesh, K., Gopalarathnam, A., Granlund, K., Ol, M. V., and Edwards, J. R., "Discrete-Vortex Method with Novel Shedding Criterion for Unsteady Aerofoil Flows with Intermittent Leading-Edge Vortex Shedding," *Journal of Fluid Mechanics*, Vol. 751, July 2014, pp. 500–538. https://doi.org/10.1017/jfm.2014.297

[22] Ramesh, K., Granlund, K. O., Ol, M. V., Gopalarathnam, A., and Edwards, J. R., "Leading-Edge Flow Criticality as a Governing Factor in Leading-Edge Vortex Initiation in Unsteady Airfoil Flows," *Theoretical and Computational Fluid Dynamics*, Vol. 32, No. 2, 2018, pp. 109–136. https://doi.org/10.1007/s00162-017-0442-0

[23] Saini, A., and Gopalarathnam, A., "Leading-Edge Flow Sensing for Aerodynamic Parameter Estimation," *AIAA Journal*, Vol. 56, No. 12, 2018, pp. 4706–4718. https://doi.org/10.2514/1.J057327

[24] Hou, W., Darakananda, D., and Eldredge, J. D., "Machine-Learning-Based Detection of Aerodynamic Disturbances Using Surface Pressure Measurements," *AIAA Journal*, Vol. 57, No. 12, 2019, pp. 5079–5093. https://doi.org/10.2514/1.J058486

[25] Deparday, J., and Mulleners, K., "Modeling the Interplay Between the Shear Layer and Leading Edge Suction During Dynamic Stall," *Physics of Fluids*, Vol. 31, No. 10, 2019, Paper 107104. https://doi.org/10.1063/1.5121312

[26] Bergh, H., and Tijdeman, H., "Theoretical and Experimental Results for the Dynamic Response of Pressure Measuring Systems," National Aerospace Lab./NLR TR NLR-TR F.238, Amsterdam, 1965, https://repository.tudelft.nl/islandora/object/uuid%3Ae88af84e-120f-4c27-8123-3225c2acd4ad.

[27] Ewald, B., "Wind Tunnel Wall Corrections," AGARDograph Rept. AGARD-AG-336, Neuilly-Sur-Seine, France, 1998.

[28] Evans, W. T., and Mort, K. W., "Analysis of Computed Flow Parameters for a Set of Sudden Stalls in Low-Speed Two-Dimensional Flow," NASA TN D-85, 1959.

[29] James, E. C., "Leading Edge Separation Criterion for an Oscillating Airfoil," *Workshop on Unsteady Separated Flow*, Air Force Office of Scientific Research, AD-P004 175, Boiling AFB, D.C., 1983. https://doi.org/10.21236/adp004175

[30] Harms, T., Nikoueeyan, P., and Naughton, J. W., "An Experimental Evaluation of Cycle-to-Cycle Variations of Dynamic Stall," AIAA Paper 2018-1267, 2018. https://doi.org/10.2514/6.2018-1267

[31] Smith, M. J., Jones, A. R., Ayancik, F., Mulleners, K., and Naughton, J. W., "An Assessment of the State-of-the-Art from the 2019 ARO Dynamic Stall Workshop," AIAA Paper 2020-2697, 2020. https://doi.org/10.2514/6.2020-2697

[32] Mulleners, K., and Raffel, M., "Dynamic Stall Development," *Experiments in Fluids*, Vol. 54, No. 2, 2013, pp. 1469–1477. https://doi.org/10.1007/s00348-013-1469-7

[33] Houghton, E., Carpenter, P., Collicott, S. H., and Valentine, D. T., "Chapter 6—Thin Airfoil Theory," *Aerodynamics for Engineering Students*, 7th ed., Butterworth-Heinemann, Oxford, England, U.K., 2017, pp. 391–447. https://doi.org/10.1016/B978-0-08-100194-3.00006-7

K. Taira
Associate Editor